Molecular Catalysis 595 (2026) 115847

Contents lists available at ScienceDirect

Molecular Catalysis

journal homepage: www.journals.elsevier.com/molecular-catalysis

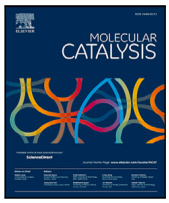

Research paper

Oxygen evolution reaction on Pt supported maghemite surfaces

Amit Sahu [a], Sung Sakong [b], Axel Gross [b], Céline Dupont [a,*]

[a] Laboratoire Interdisciplinaire Carnot de Bourgogne (ICB), UMR 6303 CNRS, Université Bourgogne Europe, BP 47870, Dijon Cedex, 21078, France
[b] Institute of Theoretical Chemistry, Ulm University, Oberberghof 7, Ulm, 89081, Germany

ARTICLE INFO

Keywords:
γ-Fe_2O_3
Oxygen evolution reaction
Strain effect
DFT

ABSTRACT

Maghemite surfaces have recently emerged as promising materials for (electro)photo-catalytic applications, particularly in the context of the oxygen evolution reaction (OER). In this study, density functional theory (DFT) is applied to explore the mechanistic details of OER and its fundamental steps on the most stable maghemite layers grown on a Pt substrate. Our investigation reveals that the Pt substrate significantly influences the surface energetics, through both geometric and electronic effects. On the (001) surface, the geometry of Pt negatively affects the OER energetics. On the contrary, the inclusion of electronic effects facilitates the evolution of oxygen, however, energetics remains less favorable than on the free standing surface. A comparative analysis of the (001) and (111) maghemite surfaces demonstrates that both surfaces present a similar reactivity towards OER, when grown on a Pt substrate. In particular, an overpotential (η) of 1.28 V is calculated on the (111) surface, a value similar to that on (001) (η = 1.30 V). Despite a similar global reactivity, distinct potential limiting steps are identified. Specifically, on the (111) surface, the formation of the *OH intermediate is identified as the potential limiting step, while the *O formation is limiting on the (001) surface, as commonly observed on other iron oxides. These findings offer atomic-level insights about the reactivity of maghemite surfaces over OER process. They also clearly evidence the influence of surface structure on mechanisms and that of substrate on global efficiency.

1. Introduction

Iron oxides are among the most important environmentally friendly materials owning a large number of applications. The interaction of water with iron oxide surfaces is the core mechanism in numerous areas, like geochemistry, corrosion, catalysis, or electrochemistry [1–6]. Especially, in these fields, maghemite is one of the iron oxides that attracts significant attention since recent years. Up to now, it has been under investigation through a surface science approach, both as nanoparticles [7] and supported thin films [8–10] in vacuum due to its diversified applications ranging from biomaterial [11], pollutant removal [12–14], magnetic data storage [15] to catalysis [16–19]. Therefore, inclusion of the interaction of water with iron oxide surfaces is important to have a complete understanding of their role in key electrocatalytic processes.

In general, the interaction of water with iron oxide surfaces is an extensively studied phenomenon. The wide interaction of hematite with water is well known. Both entirely theoretical [20,21] and combined [22–24] studies have evidenced either the spontaneous dissociative adsorption or molecular adsorption, rapidly followed by dissociation with low activation barriers. Concerning magnetite, favored interaction with water has also been demonstrated, with some nuances depending on the termination. While highly exothermic dissociative adsorption has been mainly observed on Fe_3O_4(111) [25,26], partial dissociation [27] and molecular adsorption can also occur on Fe_3O_4(001) [28,29]. However, within our knowledge, no in-depth studies have been performed to elucidate the interaction between water and maghemite, despite some evidence [30,31] of a substantial interaction. Besides, the oxygen evolution reaction has been explored in detail on both hematite [32–35] and magnetite [36–39]. Still, despite some evidence of the important ability of maghemite for oxygen evolution reactions [40] and its promising applications in water-splitting [41–43], only few studies explored water splitting on maghemite surfaces due to its complex surface structure and ferrimagnetic nature [41,42,44,45]. Hence, an atomic-scale theoretical insight into OER, its intermediates, and reactive sites on maghemite surfaces is necessary to explore its applicability. This is all the more crucial that the mechanism of OER is widely influenced by the surface structure of the oxide, as identified in the numerous studies about OER on metal oxides [46,47]. Hence, it is worth determining if the particular structure of maghemite can play a role in improving OER efficiency.

To do so, the mechanism of OER is investigated on maghemite first in acidic conditions, as already done on hematite [34,48], for example.

* Corresponding author.
E-mail addresses: axel.gross@uni-ulm.de (A. Gross), celine.dupont@u-bourgogne.fr (C. Dupont).

https://doi.org/10.1016/j.mcat.2026.115847
Received 5 January 2026; Received in revised form 24 February 2026; Accepted 2 March 2026

In these conditions, bare maghemite will be considered. Indeed, given its high polarity, maghemite is naturally easily hydroxylated. However, in acidic conditions, protons react with surface hydroxyls to restore native surface. Besides, iron oxides, as well as other metal oxides, are rarely used alone, but often deposited on substrates, like for example, hematite on Pt(111) for solar water splitting [49], or thin films of FeO(111) on Au(111) or Pt(111) for CO oxidation [50]. As evidenced, among others, by Grave et al. [51], for hematite deposited on Pt(111), the presence of the substrate has two main interests. Firstly, epitaxial growth on a single Pt(111) substrate allows the obtention of a well-defined and reproducible crystallographic structure for the top thin films [49]. Secondly, a metallic substrate allows bottom conductive contact, essential for efficient electrochemical measurements [52,53]. For maghemite, the use of a substrate is all the more crucial as bulk maghemite is not stable and thus maghemite exists only as nanoparticles or films grown on a substrate. Nevertheless, if the presence of the substrate brings real added values for model studies, it also has a non-negligible influence on reactivity. Hence, several studies of OER catalyzed by metal oxides have evidenced the influence of the substrate. For example, different behaviors have been demonstrated for CoO_x deposited either on Ir(111) or on Pt(111) [54] or for RuO_2 deposited on different materials like platinum, titanium, nickel or glassy carbon [55]. The choice of the substrate can thus influence further reactivity. Given previous results suggesting maghemite-Pt composites as promising catalysts [56], but also the conductive nature of platinum and the fact that it allows well-defined epitaxial growth [49], a platinum substrate has been chosen in the following.

Thus, it appears mandatory to also consider the role of the substrate, in our case platinum, when investigating OER mechanism on maghemite. As a consequence, in this work, the interaction of water molecules with the most stable terminations of Pt supported maghemite (001) and (111) surfaces is firstly considered. After a probe study to determine the most stable adsorption sites, the oxygen evolution reaction (OER) is investigated. Different levels of calculations are considered to investigate the geometric and electronic role of the substrate. Finally, the required overpotential for the different cases is compared.

2. Model structures and computational methods

2.1. Computational details

All calculations have been performed using the Vienna ab-initio simulation package (VASP 5.4.4) [57,58] based on plane-wave density functional theory (DFT). As maghemite displays a ferrimagnetic nature, calculations with the consideration of spin-polarized effects are performed. We initialized the magnetic moments, *i.e.*, +5 μB for octahedral iron atoms and −5 μB for tetrahedral ones, to correctly reproduce their bulk values, +4 μB and −4 μB, for the iron atoms in the middle of the slab. A summary of final magnetic moments is given in SI. Projector-augmented plane-wave (PAW) method [59] is employed with eight valence electrons for Fe ($3d^74s^1$), six for O ($2s^22p^4$), and ten for Pt ($5d^96s^1$). The Perdew, Burke and Ernzerhof (PBE) exchange–correlation functional is applied within the framework of the general gradient approximation (GGA) [60] to account exchange–correlation interactions. To consider the long-range interactions, Grimme D3 (DFT-D3) dispersion correction is used with zero damping [61], while the bandgap issue is solved applying the DFT+U Dudarev approach [62]. A value of 4.3 eV is considered for U_{eff}, leading to a favorable alignment with experimental bulk properties [63,64]. The Brillouin zone sampling is done using a Monkhorst–Pack k-point mesh, the accuracy of which depends on the cell size. Gaussian smearing with a width of 0.1 is employed to improve convergence and minimize electronic energy. The kinetic energy cutoff of the plane-wave basis is set at 550 eV, and convergence thresholds for energy and forces are established at 10^{-5} eV and 0.02 eV/Å, respectively.

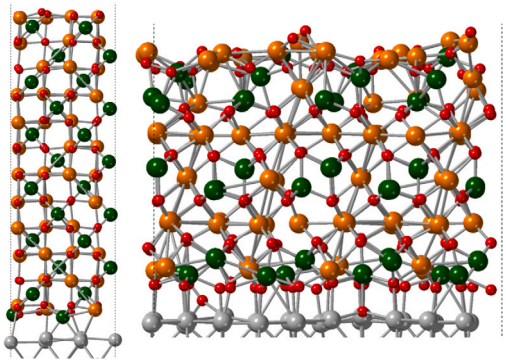

Fig. 1. Side views of the two most stable surfaces of maghemite adsorbed on platinum. (Left) AB(001) from tetragonal model (Right) EF(111) from cubic model. Tetrahedral iron atoms (Fe_{Th}) are reported in green, octahedral ones (Fe_{Oh}) in orange and oxygen atoms in red. More details about these structures can be found in [65].

2.1.1. Model structures

Following our previous work [65], we only considered the two most stable surfaces of Pt supported maghemite, namely AB (001) from the tetragonal model and EF (111) from the cubic one (see Fig. 1).

The cell size for AB(001)/Pt is 8.32 × 8.32 × 53.77 Å, including a vacuum of 19 Å and corresponding to a 0.84% constraint on maghemite along x and y directions, induced by the lattice mismatch between maghemite and Pt substrate as original cell corresponds to 8.39 × 8.39 Å along x and y directions. Similarly, cell parameters for EF are equal to 19.60 × 11.76 × 49.00 Å, corresponding to a vacuum of 23 Å and a constraint of 0.86% along x and 4.64% along y direction as the original cell corresponds to 20.55 × 11.87 Å in the x and y direction. To sample the Brillouin zone, Monkhorst–Pack k-point meshes are chosen according to cells' sizes. Hence, a 4 × 4 × 1 Monkhorst–Pack k-point mesh is used for the AB termination and a 2 × 4 × 1 for the EF.

In the following, three different cases for the AB and EF cells will be considered in order to understand how the platinum substrate influences the OER energetics on the AB and EF surfaces. The geometrical contribution of Pt and the combination of both geometrical and electronical influences of Pt will be investigated with the three cases depicted in Fig. 2. First, the free standing maghemite surface is considered. Secondly, only the geometrical effect of platinum is introduced by straining maghemite layer to the Pt lattice parameters, but without explicit Pt support. Practically, the structure of maghemite is extracted from the previously optimized γ-Fe_2O_3/Pt system [65]. In water adsorption on this strained maghemite, only the top 5 layers are allowed to relax. Finally, the five layers Pt substrate itself is introduced, with only the top 5 layers of maghemite allowed to relax (see Fig. 2). This would allow us to decouple the geometric and electronic influence of Pt substrate over OER reaction intermediates.

2.2. Energetics of reaction intermediates

To analyze water adsorption on the different surfaces, we calculate its adsorption energy (E_{ads}) using the following formula:

$$E_{\text{ads}}(\gamma - Fe_2O_3) = E_{H_2O@\gamma-Fe_2O_3} - E_{H_2O} - E_{\gamma-Fe_2O_3} \quad (1)$$

$$E_{\text{ads}}(\gamma - Fe_2O_3/Pt) = E_{H_2O@\gamma-Fe_2O_3/Pt} - E_{H_2O} - E_{\gamma-Fe_2O_3/Pt} \quad (2)$$

This allows us to quantify and comprehend the binding strength between water molecules and the various surfaces under consideration.

In acidic conditions, water oxidation is given by the following equation:

$$2H_2O \rightarrow O_{2\ (gas)} + 4H^+ + 4e^- \ ; \ \Delta G_0 = 4.92\ eV \quad (3)$$

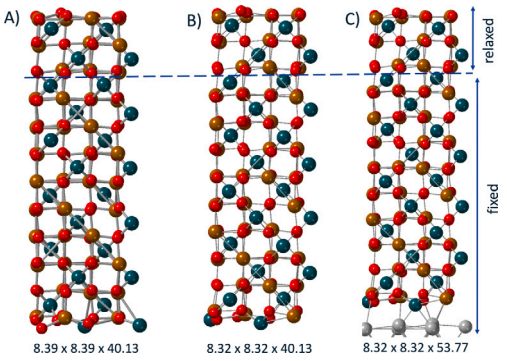

Fig. 2. The three considered cases for OER energetics: (A) Native γ-Fe_2O_3, without any influence of platinum, (B) with geometrical influence of Pt, namely γ-Fe_2O_3 constrained to the lattice parameter of platinum, with geometry extracted from γ-Fe_2O_3/Pt and (C) with both geometric and electronic influences of Pt (only top 5 layers are relaxed).

The water oxidation is assumed to take place in four elementary steps:

$$* OH \rightarrow * O + H^+ + e^- \quad (4)$$

$$* O + H_2O \rightarrow * OOH + H^+ + e^- \quad (5)$$

$$* OOH \rightarrow * OO + H^+ + e^- \quad (6)$$

$$* OO + H_2O \rightarrow O_{2(gas)} + * OH + H^+ + e^- \quad (7)$$

The free energy change (ΔG) for each step can be determined through the following expression:

$$\Delta G = \Delta E + \Delta ZPE - T\Delta S \quad (8)$$

Entropic contributions for adsorbed species are usually minimal due to a very limited degree of freedom, therefore, they will be neglected in the following, as often applied for both OER [66,67] and HER [68,69]. The ZPE correction of adsorbed species was neglected. On the contrary, the gas-phase thermal corrections of molecules were taken from ref [37], while vibration corrections having, in general, more impact on transition states, are out of the scope of the current study.

To be able to make a link with experimental studies, we have used the computational hydrogen electrode (CHE) approach as suggested by Nørskov and co-workers [70]. Even if this approach presents several limitations due to its intrinsic hypotheses [71,72], it has already been successfully applied in numerous cases [32,33,39], allowing an efficient and reasonable overview, within a low computational cost. The CHE approach is thus based on the fact that the sum of the chemical potentials of protons and electrons at pH = 0 and at zero applied bias on the standard hydrogen electrode (SHE) scale is equal to the chemical potential of gas-phase hydrogen under standard conditions. The effect of external potential is applied only to the chemical potential of the electrons by $-eU$, where e is the electronic charge [73]. Hence, with the SHE electrode as reference, the free energies of OER elementary steps [74] are calculated with the following equations:

$$\Delta G_1 = E_{*O} + \frac{1}{2}E_{H_2} - E_{*OH} - \frac{1}{2}(T\Delta S_{H_2} - \Delta ZPE_{H_2}) - eU_{SHE} \quad (9)$$

$$\Delta G_2 = E_{*OOH} + \frac{1}{2}(E_{H_2} - \Delta ZPE_{H_2}) - E_{*O} - E_{H_2O(l)} + T\Delta S_{H_2O} - \frac{1}{2}T\Delta S_{H_2} - eU_{SHE} \quad (10)$$

$$\Delta G_3 = E_{*OO} + \frac{1}{2}(E_{H_2} - \Delta ZPE_{H_2}) - E_{*OOH} - \frac{1}{2}T\Delta S_{H_2} - eU_{SHE} \quad (11)$$

$$\Delta G_4 = E_{*OH} - E_{*OO} + E_{H_2O(l)} - \frac{3}{2}(E_{H_2} - \Delta ZPE_{H_2}) - T\Delta S_{H_2O} + \frac{3}{2}T\Delta S_{H_2} - \Delta G_0 - eU_{SHE} \quad (12)$$

Adding all the elementary free energies would result into the following global free energy:

$$\Delta G_1 + \Delta G_2 + \Delta G_3 + \Delta G_4 = \Delta G_0 - 4eU_{SHE} \quad (13)$$

Table 1
Adsorption energies (in eV) of water on the four octahedral iron (States A, B, C and D) for the three considered cases for AB(001): free standing surface, maghemite with Pt strain, maghemite on Pt. Associated magnetic moments in μ_B per Fe_2O_3 unit are reported in parenthesis for each case.

E_{ads} (μ)	(A)	(B)	(C)	(D)
Free standing	−0.46 (2.46)	−0.56 (2.46)	−0.69 (2.46)	−0.64 (2.47)
Pt geometry	−0.60 (2.47)	−0.38 (2.42)	−0.64 (2.46)	−0.45 (2.46)
On Pt	−1.72 (2.47)	−0.77 (2.38)	−0.65 (2.38)	−0.62 (2.38)

To characterize activity of the different systems, limiting potential ($U_{limiting}$), defined as the applied specific potential where all steps are neutral or exothermic, will be use. In this case, we approximated the applied potential when OER energetics becomes thermodynamically favorable. Finally, we will also consider overpotential (η), defined as the difference between the actual required voltage and the theoretical half-cell reaction voltage. In order to calculate the required overpotential, the following equation has been used:

$$\eta = \frac{1}{e}max[\Delta G_n] - 1.23\ V \quad (14)$$

3. Results

The effect of a platinum substrate on water adsorption, and more generally on OER energetics is analyzed, firstly from the geometrical aspect alone, then from combined geometrical and electronic influences. To do so, the AB(001) termination in the tetragonal structure [65] is considered within the three models described in computational details, namely free standing γ-Fe_2O_3, strained γ-Fe_2O_3 (geometrical effect of Pt) and γ-Fe_2O_3/Pt (geometrical and electronic effects of Pt). Then, the second part deals with adsorption of OER intermediates and respective OER energetics on EF(111) from the cubic model. Finally, reaction intermediates, potential limiting steps, and required overpotentials are compared for both (001) and (111) terminations.

3.1. Adsorption of water on AB surface

Water adsorption is firstly probed on free standing AB(001). Given the top layer obtained for maghemite grown on Pt, namely B layer (see Fig. 1), adsorption of water is only considered on the B side of the slab. B layer is composed of octahedral iron atoms (Fe_{Oh}), while underneath tetrahedral iron Fe_{Th} are not accessible for water adsorption. Considering water adsorption on all four Fe_{Oh} of the top layer leads to adsorption energies ranging from −0.38 to −0.69 eV (see Table 1), associated with geometries reported in Fig. 3 and in SI. The range of molecular water adsorption energies is in agreement with previous theoretical studies performed on other iron oxide surfaces [37].

Even if water molecules are slightly tilted (see Fig. 3), the interaction of hydrogen atoms with O atom from the surface is not sufficient to lead to substantial hydrogen bonds able to increase the stability.

Next, the geometrical influence of platinum inducing strain effects is considered, leading to various behaviors. While strain has almost no influence on (C) state, it stabilizes (A) state, this latter becoming competitive with (C) (E_{ads} = −0.60 and −0.64 eV, respectively). On the contrary, strain destabilizes both (B) and (D) states in a similar extent. One has to mention that the geometrical impact of Pt reduces the intrinsic stability of maghemite surface due to the fixed geometry imposed by Pt interaction, leading to a different reactivity of the surface towards water. Finally, in presence of Pt, the adsorption energy increases for (A), (B), and (D) states, while energy of (C) remains almost constant. This increase is clearly more important for (A) state than for the others. This is directly related to the magnetic moment. Indeed, when Pt is explicitly introduced, the magnetic moment keeps a value close to the experimental one of 2.5 μ_B/Fe_2O_3[75], while it decreases to 2.38 μ_B for the other configurations. The magnetic destabilization

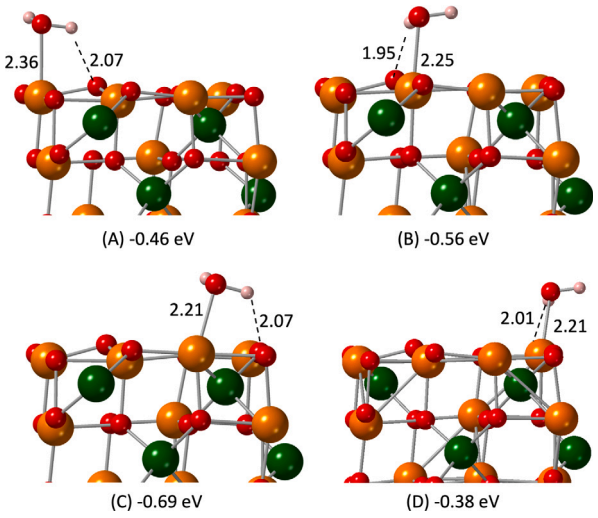

Fig. 3. Lateral views of water adsorbed on bare AB(001), on the four available octahedral sites. Adsorption energies are reported in eV, while useful bond lengths are specified in Å. Corresponding top views are reported in SI.

compensates stabilization by Pt substrate, thus reducing its effect. These results demonstrate that, despite the computational cost, the complete influence, namely geometric and electronic, of Pt substrate has to be considered when studying the interaction of water with maghemite.

3.2. Adsorption of OER intermediates

Following the preliminary step of water adsorption, adsorption of all other OER intermediates has been considered on the three systems mentioned above in order to identify Pt substrate influence on the kinetics and potential limiting steps of the OER reaction energy profile. Intermediates have been considered within the adsorbate evolution mechanism (AEM). However, alternative reaction pathways exist, such as lattice-oxygen mediated or oxide-path mechanisms. AEM has been chosen because it is the most common and widely accepted pathway for OER on oxide surfaces, in particular, on defect- and vacancy-free, such as the pristine maghemite considered in this study. Hence, in this mechanism, OER elementary steps involve *OH (hydroxyl), *O (oxo), *OOH (hydroperoxo), and *OO (superoxo) intermediates (see Fig. 4 and SI). Hence, the Gibbs free energy for these different elementary steps has been calculated, as described in the energetics section.

All the free energies are calculated with reference to the standard hydrogen electrode (SHE), while η is calculated as the difference between the limiting potential and thermodynamic potential. The chosen reference to calculate OER energetics is the adsorbed hydroxyl (*OH) group on the surface.

3.2.1. OER energetics on γ-Fe_2O_3 - AB(001)

Initially (pH = 0, U = 0 V), all steps of oxygen evolution reaction are endothermic (see Fig. 5A black). In particular, the dehydrogenation of the hydroxyl group (step 1) and desorption of O_2 followed by the recovery of this adsorbed hydroxyl (step 4) are the most energy-demanding, with free energy changes (ΔG) of 2.12 eV and 2.15 eV, respectively. At thermodynamic potential U = 1.23 V (see Fig. 5A red), namely when the overpotential is zero (η = 0 V), *OOH and *OO formations become exothermic, while *O and *OH formations remain endothermic. However, their free energy changes are significantly reduced, with ΔG_1 = 0.89 eV and ΔG_4 = 0.92 eV. This indicates that an overpotential is needed for the overall process to be thermodynamically favorable. The required overpotential is η = 0.92 V, corresponding to a limiting potential of 2.15 V (see Fig. 5A green).

Table 2
Free energy changes (in eV) in the OER elementary steps on (001) and (111) surfaces at U = 0 V.

Free energy	AB(001)			EF(111)
changes	Native	Strained	Pt/Fe_2O_3	Pt/Fe_2O_3
ΔG_1	2.12	2.72	2.53	−0.12
ΔG_2	0.31	−0.32	0.23	1.46
ΔG_3	0.35	0.83	0.62	1.07
ΔG_4	2.15	1.69	1.54	2.51

One has to mention that these results are consistent with previous findings on other iron oxide surfaces. Indeed, previous studies on magnetite [37] or on hematite [35] have also evidenced *O formation as the potential limiting step (except for (100) termination of hematite). In those studies, overpotential of 0.67 V has been calculated for Fe_3O_4(0001), and values between 0.78 V and 1.77 V for the different terminations of hematite [34,48,76–78]. Hence, overpotential of maghemite appears to be higher than that of magnetite but is in the range of those calculated for hematite (see Table 2).

3.2.2. OER energetics on strained γ-Fe_2O_3 - AB(001)

When considering the geometrical influence of platinum (strained maghemite), the study reveals notable changes compared to the native AB(001) surface (see Fig. 5B). At pH = 0 (relative to SHE), *OOH formation becomes exothermic on the strained surface, in contrast with the native surface, where all steps were endothermic. The other elementary steps on the strained surface remain endothermic. It is important to note that the strain effect is not uniform across all intermediates. For instance, *O formation on the strained surface requires a higher free energy (ΔG_1 = 2.72 eV) than on the native surface (2.12 eV). Conversely, the endothermicity of *OH formation decreases from 2.15 eV (native) to 1.69 eV (strained). Consequently, *O formation becomes the sole potential limiting step on the strained surface.

As on the native surface, at the thermodynamic potential (U = 1.23 V, η = 0 V), both formations of *OOH and *OO become exothermic on the strained surface, while *O and *OH formations are still endothermic. Dehydrogenation of the hydroxyl group (*O formation) remains the potential limiting step with ΔG_1 = 1.49 eV, a higher value compared to native surface (ΔG_1 = 0.89 eV). Ultimately, an overpotential of η = 1.49 V (corresponding to a limiting potential $U_{limiting}$ = 2.72 V) is required to make all reaction steps thermodynamically favorable on the strained surface. This is significantly higher than the η = 0.92 V needed for the native AB(001) surface.

3.2.3. OER energetics on Pt/γ–Fe_2O_3 - AB(001)

Finally, considering the entire system with explicit Pt substrate, namely including both its geometric and electronic influences, reveals further insights. Initially, all elementary steps are endothermic, as on the native AB surface. *O formation is still the potential limiting step (ΔG_1 = 2.53 eV), exhibiting an energy requirement between that of native (2.12 eV) and strained AB (2.72 eV) systems. A key difference from the strained-only case is that *OOH formation is now endothermic, similarly to the native AB behavior.

When the thermodynamic potential of U = 1.23 V (η = 0 V) is selected, the behavior is similar to strained AB, with both *OOH and *OO formations being exothermic. Again *O and *OH formations remain endothermic and *O formation is still the potential limiting step (ΔG_1 = 1.30 eV). Therefore, an overpotential of 1.30 V (corresponding to a limiting potential $U_{limiting}$ = 2.53 V) is required to make *O formation (and thus the entire reaction pathway) thermodynamically favorable. This overall behavior – without or with potential – is intermediate between those observed for the native and strained AB systems.

According to the above results, the geometric influence of Pt increases the overpotential of the OER on maghemite. On the contrary,

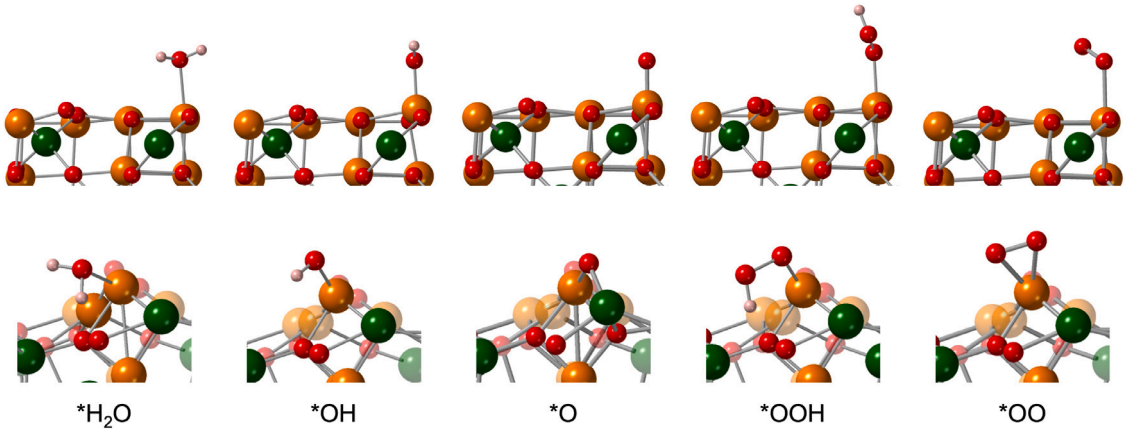

Fig. 4. Intermediates involved in the OER mechanism on γ-Fe_2O_3/Pt for (Top) tetragonal AB(001) and (Bottom) cubic EF(111). For the sake of clarity, only top three layers are reported for AB cases, while a focus on the active site (with background atoms shaded) is done for intermediates on EF. Top views for intermediates on AB(001) and larger side and top views for intermediates on EF(111) are available in SI.

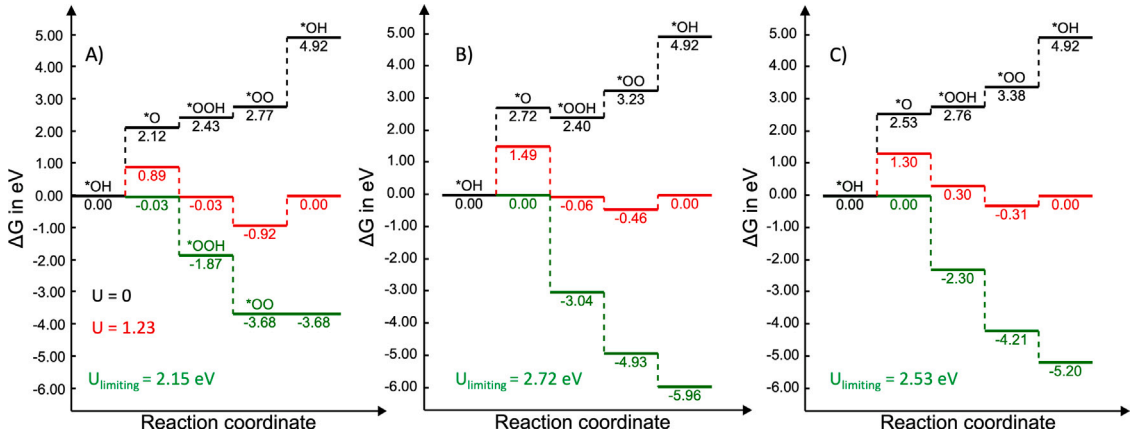

Fig. 5. OER reaction intermediates of three different cases: (A) without any effect of Pt, (B) geometric effect of Pt substrate, (C) geometric and electronic effect of Pt substrate. Black: U = 0 V, red: U = 1.23 V ($\eta = 0$ V), green: required $U_{limiting}$ (η)

when the electronic influence is also included, a slight improvement is observed. Nevertheless, even with this improvement, the resulting overpotential remains higher than that of native AB maghemite. Most importantly, this study demonstrates that the platinum substrate affects the system through both geometrical constraints and electronic interactions associated with the metallic nature of Pt. As a result, explicitly including the substrate in the model is essential, despite the added computational cost. Consequently, the following comparison of OER energetics between tetragonal and cubic maghemite models will focus solely on the γ-Fe_2O_3/Pt system, which accounts for the complete influence of Pt substrate.

3.2.4. OER energetics of γ-Fe_2O_3/Pt - AB (001) versus EF (111)

The influence of the maghemite model on the energetics of water oxidation can now be addressed, by directly considering the complete platinum/maghemite system. Before anything else, a specific methodological aspect has to be mentioned. For this surface of cubic model, a favorable adsorption site for water that also preserved the appropriate magnetic configuration could not be successfully identified. Nevertheless, the magnetic configurations of the subsequent OER steps were found to be consistent with one particular water adsorption scenario. This consistency permitted the investigation of OER energetics. The obtained results are reported in Fig. 6, together with data for the tetragonal AB(001) surface.

At first glance, the behavior of EF(111) clearly differs from that of AB(001). Indeed, while all steps are endothermic on AB(001) at U = 0 V, the *O formation step – the potential limiting step on AB(001) – is exothermic on the cubic EF(111) surface, with $\Delta G_1 = -0.12$ eV. This difference can be attributed to the adsorption geometry of the *O intermediate. On AB(001), *O adsorbs in a top position, whereas the inherent roughness of the EF(111) surface enables a bridge-like adsorption configuration, which stabilizes the *O intermediate (see Fig. 4), through two iron-oxygen bonds.

The potential limiting step on EF(111) is now the last step of desorption of O_2 followed by *OH recovery, with free energy change of $\Delta G_4 = 2.51$ eV. This change is, again, attributable to the geometry of the intermediates. Specifically, the *OO intermediate is more stabilized on the EF(111) surface because both its oxygen atoms bond with Fe atoms, unlike on AB(001), where only one oxygen interacts with an iron atom. Consequently, breaking this *OO intermediate to recover *OH is more energetically costly on the EF(111) surface. It is also noteworthy that *OOH formation, previously the most favorable step on AB(001) with $\Delta G_2 = -0.32$ eV, now exhibits a relatively high free energy change of $\Delta G_2 = 1.46$ eV on EF(111). When applying the thermodynamic potential of U = 1.23 V, *OOH formation is still endothermic, but with a low required energy of $\Delta G_2 = 0.23$ eV, while *OH remains the potential limiting step with $\Delta G_4 = 1.28$ eV. This corresponds to a significant reduction compared to U = 0 V ($\Delta G_4 = 2.51$ eV). Thus, this leads to an overpotential of 1.28 V to achieve a fully exothermic reaction pathway. This value is similar to that observed for the tetragonal AB(001) surface, where the overpotential is 1.30 V. Nevertheless, these two equivalent values are obtained with completely different potential

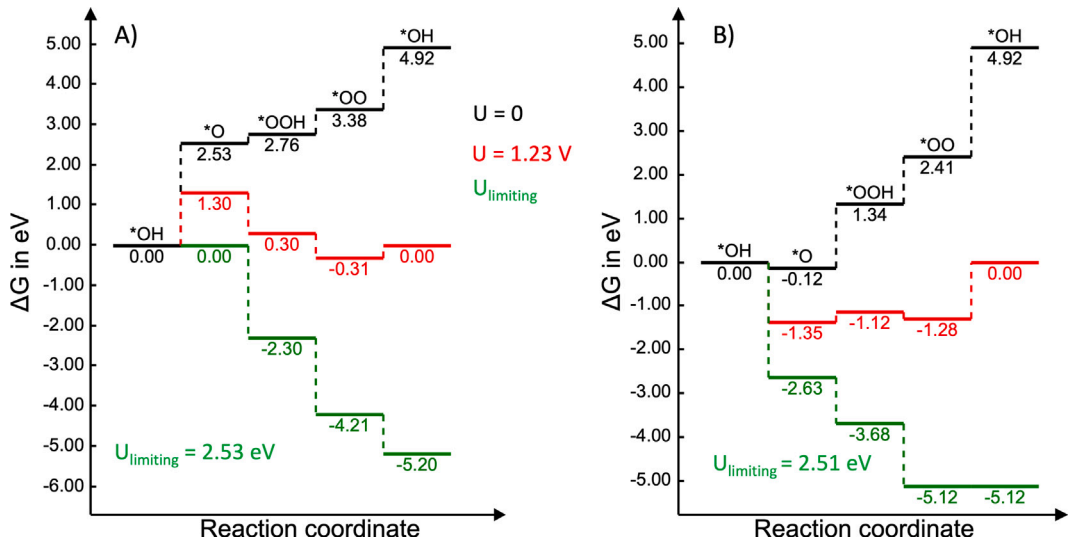

Fig. 6. OER energetics for (A) tetragonal AB(001) and (B) cubic EF(111) maghemite surfaces supported on Pt substrate. Black curve corresponds to U = 0 V, red one to U = 1.23 V ($\eta = 0$ V) and green at required $U_{limiting}$, namely η = 1.30 or 1.28 V for AB(001) and EF(111), respectively.

limiting steps. This means that ways to improve maghemite efficiency will probably differ depending on the considered model.

Finally, this study clearly demonstrates the significant impact of the substrate from both geometric and electronic contributions to electrocatalytic reactions on thin oxide films coated on a substrate. We note that overpotentials obtained on bare maghemite fit very well with values in the literature for bare hematite [35,48,76–78], while the inclusion of the substrate has a significant impact on the overpotentials. Given the necessity of a substrate in the experimental setup [51,79], taking it into consideration appears mandatory in theoretical modelings, even if at first glance it leads to relatively high overpotentials. Since previous studies [33,50,55,80] have already demonstrated the synergetic effect when platinum and metal oxides are coupled for catalysis, the effect of platinum on OER on maghemite does not seem, *a priori*, positive, given high final overpotentials. Nevertheless, this result evidences the necessity to explicitly include the substrate, but also the influence of the surface structure on mechanisms at the atomic level. Hence, screening influence of other substrates for OER on maghemite appears as interesting investigations to improve its efficiency.

4. Conclusion

In summary, the influence of maghemite structure on OER efficiency is investigated using DFT calculations. To do so, clean maghemite surfaces oriented along the (001) and (111) planes, both epitaxially grown on a Pt substrate, are considered. The account of three scenarios – free standing, strained to Pt lattice and grown on Pt – for tetragonal AB(001) maghemite, indicates that the platinum substrate plays a considerable role both with respect to geometrical and electronical effects, forcing us to consider the whole system, despite the computational cost. Due to the influence of Pt, the adsorption strength of water on the AB(001) surface is enhanced almost threefold relative to the free standing surface. Concerning the efficiency towards OER, an overpotential of 0.92 V has been calculated for free standing maghemite, a value in the range of published overpotentials for hematite. Nevertheless our study clearly evidences the effective influence of the substrate, demonstrating the potential interest to investigate other substrates.

Coming back to the complete γ-Fe_2O_3/Pt system, the nature of the termination ((001) vs (111)) changes the detailed mechanism at the atomistic level. Indeed, while *O formation is the potential determining step on tetragonal AB(001), like commonly observed on other iron oxides, this step is favored on cubic EF(111), leading to *OH formation as the determining step. These differences in potential limiting steps open the door for further investigations allowing to tailor differently both structures. Besides, overall energetics of other intermediates also change significantly. However, at the end, a minor difference is observed for overpotentials, with values of 1.28 V and 1.30 V for EF(111) and AB(001), respectively. As a consequence, this study demonstrates the potential efficiency of maghemite for OER, but above all it evidences the necessity to explicitly include the substrate in this kind of study. Finally, the differences of mechanisms at the atomic level between both models of maghemite and the significant role of the substrate pave the way to various studies to improve maghemite efficiency.

CRediT authorship contribution statement

Amit Sahu: Writing – original draft, Data curation. **Sung Sakong:** Writing – review & editing, Supervision, Resources, Methodology. **Axel Gross:** Writing – review & editing, Supervision, Resources, Methodology. **Céline Dupont:** Writing – review & editing, Supervision, Funding acquisition.

Declaration of competing interest

The authors declare that they have no known competing financial interests or personal relationships that could have appeared to influence the work reported in this paper.

Acknowledgments

This work was financially supported by the Agence Nationale de la Recherche (ANR), France project OPTYMAL, grant number ANR-20-CE42-0015-02 and ANR-17-EURE-0002 (EIPHI Graduate School). The calculations were performed at Centre de Calcul de l'Université de Bourgogne (CCuB) and IDRIS. We are thankful to the HPC resources from IDRIS under the allocation of A0130811108. We are also grateful to Bruno Domenichini for his insight and fruitful discussion on this work.

Appendix A. Supplementary data

Supplementary material related to this article can be found online at https://doi.org/10.1016/j.mcat.2026.115847.

Data availability

Data will be made available on request.

References

[1] P.A. Thiel, T.E. Madey, The interaction of water with solid surfaces: Fundamental aspects, Surf. Sci. Rep. 7 (6–8) (1987) 211–385.

[2] M. Henderson, The interaction of water with solid surfaces: fundamental aspects revisited, Surf. Sci. Rep. 46 (1–8) (2002) 1–308.

[3] E. de Smit, B.M. Weckhuysen, The renaissance of iron-based Fischer–Tropsch synthesis: on the multifaceted catalyst deactivation behaviour, Chem. Soc. Rev. 37 (2008) 2758–2781.

[4] U. Nieken A. Schüle, O. Shekhah, W. Ranke, R. Schlögl, G. Kolios, Styrene synthesis over iron oxide catalysts: from single crystal model system to real catalysts, Phys. Chem. Chem. Phys. 9 (2007) 3619–3634.

[5] A.F. White, M.L. Peterson, M.F. Hochella, Electrochemistry and dissolution kinetics of magnetite and ilmenite, Geochim. Cosmochim. Acta 58 (1994) 1859–1875.

[6] J.-Z. Wang, C. Zhong, D. Wexler, N.H. Idris, Z.-X. Wang, L.-Q. Chen, H.-K. Liu, Graphene-encapsulated Fe_3O_4 nanoparticles with 3d laminated structure as superior anode in lithium ion batteries, Chem. Eur. J. 17 (2011) 661–667.

[7] M. Nazari, N. Ghasemi, H. Maddah, M.M. Motlagh, Synthesis and characterization of maghemite nanopowders by chemical precipitation method, J. Nanostruct. Chem. 4 (2) (2014) 99/1–99/5.

[8] L.N. Lau, N.B. Ibrahim, Characterizations of maghemite thin films prepared by a sol–gel method, AIP Conf. Proc. 1678 (2015) 040013.

[9] H.-Y. Chen, S.-H. Yang, Maghemite thin films prepared using atmospheric-pressure plasma annealing, Vac. Sci. Technol. A: Vac. Surf. Films 36 (4) (2018) 04F405.

[10] M.D. Patekari, K.K. Pawar, G.B. Salunkhe, P.M. Kodam, M.N. Padvi, P. Waifalkar, K.K. Sharma, P.S. Patil, Synthesis of maghemite nanoparticles for highly sensitive and selective NO_2 sensing, Mater. Sci. Eng. B 272 (2021) 115339.

[11] M. Raman, V. Devi, M. Doble, Biocompatible l-carrageenan-γ-maghemite nanocomposite for biomedical applications –synthesis, characterization and in vitro anticancer efficacy, J. Nanobiotechnol. 13 (1) (2015) 18/1–18/13.

[12] W. Jiang, M. Pelaez, D.D. Dionysiou, M.H. Entezari, D. Tsoutsou, K. O'Shea, Chromium(VI) removal by maghemite nanoparticles, Chem. Eng. J. 222 (2013) 527–533, http://dx.doi.org/10.1016/j.cej.2013.02.049.

[13] T. Tuutijärvi, J. Lu, M. Sillanpää, G. Chen, As(V) adsorption on maghemite nanoparticles, J. Hazard. Mater. 166 (2) (2009) 1415–1420, http://dx.doi.org/10.1016/j.jhazmat.2008.12.069.

[14] A. Afkhami, R. Norooz-Asl, Removal, preconcentration and determination of Mo(VI) from water and wastewater samples using maghemite nanoparticles, Colloids Surf. A Physicochem. Eng. Asp. 346 (1) (2009) 52–57, http://dx.doi.org/10.1016/j.colsurfa.2009.05.024.

[15] E. Taboada, R.P. del Real, M. Gich, A. Roig, E. Molins, Faraday rotation measurements in maghemite-silica aerogels, J. Magn. Magn. Mater. 301 (1) (2006) 175–180.

[16] R.V. Jagadeesh, H. Junge, M. Beller, Green synthesis of nitriles using non-noble metal oxides-based nanocatalysts, Nat. Commun. 5 (1) (2014) 4123/1–4123/8, http://dx.doi.org/10.1038/ncomms5123.

[17] H. Kuhlenbeck, S. Shaikhutdinov, H.J. Freund, Well-ordered transition metal oxide layers in model catalysis - A series of case studies, Chem. Rev. 113 (6) (2013) 3986–4034, http://dx.doi.org/10.1021/cr300312n.

[18] R.V. Jagadeesh, K. Natte, H. Junge, M. Beller, Nitrogen-doped graphene-activated iron-oxide-based nanocatalysts for selective transfer hydrogenation of nitroarenes, ACS Catal. 5 (3) (2015) 1526–1529, http://dx.doi.org/10.1021/cs501916p.

[19] R.V. Jagadeesh, A.-E. Surkus, H. Junge, M.-M. Pohl, J. Radnik, J. Rabeah, H. Huan, A. Brückner V. Schünemann, M. Beller, Nanoscale Fe_2O_3-based catalysts for selective hydrogenation of nitroarenes to anilines, Science 342 (6162) (2013) 1073–1076, http://dx.doi.org/10.1126/science.1242005.

[20] S. Yin, X. Ma, D.E. Ellis, Initial stages of H_2O adsorption and hydroxylation of fe-terminated α-Fe_2O_3(0001) surface, Surf. Sci. 601 (2007) 2426–2437.

[21] M.T. Nguyen, N. Seriani, R. Gebauer, Water adsorption and dissociation on α-Fe_2O_3(0001): Pbe+u calculations, J. Chem. Phys. 138 (2013) 194709/1–194709/8.

[22] T.P. Trainor, A.M. Chaka, P.J. Eng, M. Newville, G.A. Waychunas, J.G. Catalano, G.E. Brown Jr., Structure and reactivity of the hydrated hematite (0001) surface, Surf. Sci. 573 (2004) 204–224.

[23] R. Ovcharenko L. Schöttner, A. Nefedov, E. Voloshina, Y. Wang, J. Sauer, C. Wöll, Interaction of water molecules with the α-Fe_2O_3(0001) surface: A combined experimental and computational study, J. Phys. Chem. C 123 (13) (2019) 8324–8335.

[24] P.-M. Deleuze, H. Magnan, A. Barbier, M. Silly, B. Domenichini, C. Dupont, Unraveling the surface reactivity of pristine and ti-doped hematite with water, J. Phys. Chem. Lett. 12 (47) (2021) 11520–11527.

[25] U. Leist, W. Ranke, K. Al-Shamery, Water adsorption and growth of ice on epitaxial Fe_3O_4(111), FeO(111) and Fe_2O_3 (biphase), Phys. Chem. Chem. Phys. 5 (11) (2003) 2435–2441.

[26] X. Li, J. Paier, Adsorption of water on the Fe_3O_4(111) surface: structures, stabilities, and vibrational properties studied by density functional theory, J. Phys. Chem. C 120 (2) (2016) 1056–1065.

[27] N. Mulakaluri, R. Pentcheva, M. Wieland, W. Moritz, M. Scheffler, Partial dissociation of water on Fe_3O_4(001): adsorbate induced charge and orbital order, Phys. Rev. Lett. 103 (2009) 176102/1–176102/4.

[28] X. Yu, Y. Li, Y.-W. Li, J. Wang, H. Jiao, DFT+U study of molecular and dissociative water adsorptions on the Fe_3O_4(110) surface, J. Phys. Chem. C 117 (15) (2013) 7648–7655.

[29] E. Zaki, F. Mirabella, J. Seifert F. Ivars-Barceló, S. Carey, S. Shaikhutdinov, H.-J. Freund, X. Li, J. Paier, J. Sauer, Water adsorption on the Fe_3O_4(111) surface: dissociation and network formation, Phys. Chem. Chem. Phys. 20 (23) (2018) 15764–15774.

[30] N.S. Clarke, P.G. Hall, Adsorption of water vapor by iron oxides. 2. Water isotherms and X-Ray photoelectron spectroscopy, Langmuir 7 (1991) 678–682.

[31] J. Shah, S. Jain, B. Gahtori, C. Sharma, R.K. Kotnala, Water splitting on the mesoporous surface and oxygen vacancies of iron oxide generates electricity by hydroelectric cell, Mater. Chem. Phys. 258 (2021) 123981.

[32] P. Liao, J.A. Keith, E.A. Carter, Water oxidation on pure and doped hematite (0001) surfaces: prediction of Co and Ni as effective dopants for electrocatalysis, J. Am. Chem. Soc. 134 (32) (2012) 13296–13309, http://dx.doi.org/10.1021/ja301567f.

[33] O. Neufeld, M.C. Toroker, Platinum-doped α-Fe_2O_3 for enhanced water splitting efficiency: a DFT+U study, J. Phys. Chem. C 119 (11) (2015) 5836–5847.

[34] X. Zhang, P. Klaver, R. Van Santen, M.C.M. Van De Sanden, A. Bieberle-Hütter, Oxygen evolution at hematite surfaces: the impact of structure and oxygen vacancies on lowering the overpotential, J. Phys. Chem. C 120 (32) (2016) 18201–18208.

[35] X. Zhang, C. Cao, A. Bieberle-Hütter, Orientation sensitivity of oxygen evolution reaction on hematite, J. Phys. Chem. C 120 (50) (2016) 28694–28700.

[36] M. Müllner, M. Riva, F. Kraushofer, M. Schmid, G.S. Parkinson, S.F.L. Mertens, U. Diebold, Stability and catalytic performance of reconstructed Fe_3O_4 (001) and Fe_3O_4(110) surfaces during oxygen evolution reaction, J. Phys. Chem. C 123 (13) (2019) 8304–8311.

[37] G. Righi, S. Fabris, S. Piccinin, Oxygen evolution reaction on the Fe_3O_4(001) surface: theoretical insights into the role of terminal and bridging oxygen atoms, J. Phys. Chem. C 125 (34) (2021) 18752–18761.

[38] F. Mirabella, M. Müllner, T. Touzalin, M. Riva, Z. Jakub, F. Kraushofer, M. Schmid, M.T. Koper, G.S. Parkinson, U. Diebold, Ni-modified Fe_3O_4(001) surface as a simple model system for understanding the oxygen evolution reaction, Electrochim. Acta 389 (2021) 138638.

[39] E. Bianchetti, D. Perilli, C. Di Valentin, Improving the oxygen evolution reaction on Fe_3O_4(001) with single-atom catalysts, ACS Catal. 13 (7) (2023) 4811–4823.

[40] G. Song, M. Wei, J. Zhou, L. Mu, S. Song, Modulation of the phase transformation of Fe_2O_3 for enhanced water oxidation under a magnetic field, ACS Catal. 14 (2) (2024) 846–856.

[41] W.L. Kwong, C.C. Lee, A. Shchukarev, E. Björn, J. Messinger, High-performance iron (III) oxide electrocatalyst for water oxidation in strongly acidic media, J. Catal. 365 (2018) 29–35.

[42] F. Davodi, E. Mühlhausen, M. Tavakkoli, J. Sainio, H. Jiang, B. Gökce, G. Marzun, T. Kallio, Catalyst support effect on the activity and durability of magnetic nanoparticles: toward design of advanced electrocatalyst for full water splitting, ACS Appl. Mater. Interfaces 10 (37) (2018) 31300–31311.

[43] M. Tavakkoli, T. Kallio, O. Reynaud, A.G. Nasibulin, J. Sainio, H. Jiang, E.I. Kauppinen, K. Laasonen, Maghemite nanoparticles decorated on carbon nanotubes as efficient electrocatalysts for the oxygen evolution reaction, J. Mater. Chem. A 4 (14) (2016) 5216–5222, http://dx.doi.org/10.1039/C6TA01472K.

[44] T. Tokubuchi, R.I. Arbi, P. Zhenhua, K. Katayama, A. Turak, W.Y. Sohn, Enhanced photoelectrochemical water splitting efficiency of hematite (α-Fe_2O_3)-based photoelectrode by the introduction of maghemite (γ-Fe_2O_3) nanoparticles, J. Photochem. Photobiol. A: Chem. 410 (2021) 113179, http://dx.doi.org/10.1016/j.jphotochem.2021.113179.

[45] A. Sahu, J. Parize, C. Dupont, Epitaxial growth of maghemite (001) and (111) on platinum: An ab-initio study, Appl. Surf. Sci. 630 (2023) 157467.

[46] T.R. Cook, D.K. Dogutan, S.Y. Reece, Y. Surendranath, T.S. Teets, N.D. G., Solar energy supply and storage for the legacy and nonlegacy worlds, Chem. Rev. 110 (2010) 6474–6502.

[47] M. Sotoudeh, A. Gross, Polaronic competition triggers the H_2O_2 evolution on perovskite oxides during water oxidation, ACS Catal. 15 (2025) 11544–11553.

[48] M. Nguyen, N. Seriani, S. Piccinin, R. Gebauer, Photo-oxidation of water on defective hematite(0001), ACS Catal. 5 (2015) 715–721.

[49] M. Rioult, H. Magnan, D. Stanescu, H. Barbier, Single crystalline hematite films for solar water splitting: Ti-doping and thickness effects, J. Phys. Chem. C 118 (2014) 3007–3014.

[50] X. Weng, K. Zhang, Q. Pan, Y. Martynova, S. Shaikhutdinov, F. H.J., Support effects on co oxidation on metal-supported ultrathin FeO(111) films, Chem. Cat. Chem. 9 (2017) 705–712.

[51] D. Grave, H. Dotan, Y. Levy, Y. Piekner, B. Scherrer, K. Malviya, A. Rothschild, Heteroepitaxial hematite photoanodes as a model system for solar water splitting, J. Mater. Chem. A 4 (2016) 3052–3060.

[52] G. Ketteler, W. Weiss, W. Ranke, Surface structures of α-Fe_2O_3(0001) phases determined by leed crystallography, Surf. Rev. Lett. 8 (2001) 661–683.

[53] H. Magnan, D. Stanescu, M. Rioult, E. Fonda, A. Barbier, Enhanced photoanode properties of epitaxial ti doped α-Fe_2O_3(0001) thin films, Appl. Phys. Lett. 101 (2012) 133908/1–133908/4.

[54] N. Todoroki, H. Tsurumaki, A. Shinomiya, T. Wadayama, Surface microstructures and oxygen evolution properties of cobalt oxide deposited on Ir(111) and Pt(111) single crystal substrates, Electrochem. Sci. Adv. 3 (2023) e2200007/1–e2200007/9.

[55] A. Mills, M. Browne, Determining the importance of the electrode support and fabrication method during the initial screening process of an active catalyst for the oxygen evolution reaction, J. Mater. Chem. A 6 (2018) 14162–14169.

[56] X. Teng, D. Black, N. Watkins, Y. Gao, H. Yang, Platinum-maghemite core–shell nanoparticles using a sequential synthesis, Nano Lett. 3 (2003) 261–264.

[57] G. Kresse, J. Furthmüller, Efficiency of ab-initio total energy calculations for metals and semiconductors using a plane-wave basis set, Comput. Mater. Sci. 6 (1) (1996) 15–50, http://dx.doi.org/10.1016/0927-0256(96)00008-0.

[58] G. Kresse, J. Furthmüller, Efficient iterative schemes for *ab initio* total-energy calculations using a plane-wave basis set, Phys. Rev. B 54 (1996) 11169–11186.

[59] G. Kresse, D. Joubert, From ultrasoft pseudopotentials to the projector augmented-wave method, Phys. Rev. B 59 (3) (1999) 1758–1775, http://dx.doi.org/10.1103/PhysRevB.59.1758.

[60] J.P. Perdew, K. Burke, M. Ernzerhof, Generalized gradient approximation made simple, Phys. Rev. Lett. 77 (1996) 3865–3868, http://dx.doi.org/10.1103/PhysRevLett.77.3865.

[61] S. Grimme, J. Antony, S. Ehrlich, H. Krieg, A consistent and accurate ab initio parametrization of density functional dispersion correction (DFT-D) for the 94 elements H-Pu, J. Chem. Phys. 132 (15) (2010) 154104, http://dx.doi.org/10.1063/1.3382344.

[62] S.L. Dudarev, G.A. Botton, S.Y. Savrasov, C.J. Humphreys, A.P. Sutton, Electron-energy-loss spectra and the structural stability of nickel oxide: An LSDA+U study, Phys. Rev. B 57 (1998) 1505–1509, http://dx.doi.org/10.1103/PhysRevB.57.1505.

[63] Y. Meng, X.-W. Liu, C.-F. Huo, W.-P. Guo, D.-B. Cao, Q. Peng, A. Dearden, X. Gonze, Y. Yang, J. Wang, H. Jiao, Y. Li, X.-D. Wen, When density functional approximations meet iron oxides, J. Chem. Theory Comput. 12 (10) (2016) 5132–5144.

[64] G. Rollmann, P. Entel, A. Rohrbach, J. Hafner, High-pressure characteristics of α-Fe_2O_3 using DFT+U, Phase Transit. 78 (1–3) (2005) 251–258.

[65] A. Sahu, C. Dupont, Maghemite surface termination variations: Influence of models and Pt substrate, Surf. Interfaces 55 (2024) 105377.

[66] N. Wang, A. Xu, P. Ou, S. Hung, A. Ozden, Y. Lu, J. Abed, Z. Wang, Y. Yan, M. Sun, Y. Xia, M. Han, J. Han, K. Yao, F. Wu, P. Chen, A. Vomiero, A. Seifitokaldani, X. Sun, D. Sinton, Y. Liu, E. Sargent, H. Liang, Boride-derived oxygen-evolution catalysts, Nat. Commun. 12 (2021) 6089.

[67] E. Sargeant, F. Illas, P. Rodriguez, F. Calle-Vallejo, Importance of the gas-phase error correction for O_2 when using dft to model the oxygen reduction and evolution reactions, J. Electroanal. Chem. 896 (2021) 115178/1–115178/7.

[68] N. Abidi, A. Bonduelle-Skrzypcak, S. Steinmann, How to dope the basal plane of 2H-MoS_2 to boost the hydrogen evolution reaction? Electrochim. Acta 439 (2023) 141653.

[69] N. Abidi, A. Sahu, P. Raybaud, S. Steinmann, Electrochemical potential-dependent stability and activity of MoS_3 during the hydrogen evolution reaction, ACS Catal. 13 (2023) 15290–15300.

[70] J.K. Nørskov, J. Rossmeisl, A. Logadottir, L. Lindqvist, J.R. Kitchin, T. Bligaard, H. Jónsson, Origin of the overpotential for oxygen reduction at a fuel-cell cathode, J. Phys. Chem. B 108 (46) (2004) 17886–17892.

[71] N. Govindarajan, G. Kastlunger, J. Gauthier, J. Cheng, I. Filot, A. Hagopian, H. Hansen, J. Huang, P. Kowalski, J. Liu, J. Lombardi, M. Maraschin, A. Peterson, H. Pillai, H. Prats, C. Price, R. van Roij, J. Rossmeisl, R. Seemakurthi, S. Shin, A. Smith, J. Zhu, K. Doblhoff-Dier, The intricacies of computational electrochemistry, ACS Energy Lett. 10 (2025) 4277–4288.

[72] M. Vasanthapandiyan, S. Singh, F. Bononi, O. Andreussi, N. Karmodak, Thermodynamic and kinetic modeling of electrocatalytic reactions using a first-principles approach, J. Chem. Phys. 159 (2023) 111001/1–111001/26.

[73] A. Gross, Grand-canonical approaches to understand structures and processes at electrochemical interfaces from an atomistic perspective, Curr. Opin. Electrochem. 27 (2021) 100684/1–100684/8.

[74] Q. Liang, G. Brocks, A. Bieberle-Hütter, Oxygen evolution reaction (OER) mechanism under alkaline and acidic conditions, J. Phys. Energy 3 (2) (2021) 026001.

[75] R. Dronskowski, The little maghemite story: A classic functional material, Adv. Funct. Mater. 11 (2001) 27–29.

[76] A. Hellman, R. Pala, First-principles study of photoinduced water-splitting on Fe_2O_3, J. Phys. Chem. C 115 (2011) 12901–12907.

[77] M. Nguyen, N. Seriani, S. Piccinin, R. Gebauer, Photo-driven oxidation of water on α-Fe_2O_3 surfaces: An *ab initio* study, J. Chem. Phys. 140 (2014) 064703/1–064703/8.

[78] A. Hellman, B. Iandolo, B. Wickman, H. Grönbeck, J. Baltrusaitis, Electro-oxidation of water on hematite: Effects of surface termination and oxygen vacancies investigated by first-principles, Surf. Sci. 640 (2015) 45–49.

[79] A. Bandarenka, M. Koper, Structural and electronic effects in heterogeneous electrocatalysis: Toward a rational design of electrocatalysts, J. Catal. 308 (2013) 11–24.

[80] Y. Sun, Z. Qin, M. Lewandowski, E. Carrasco, M. Sterrer, S. Shaikhutdinov, H. Freund, Monolayer iron oxide film on platinum promotes low temperature co oxidation, J. Catal. 266 (2009) 359–368.